Journal Pre-proof

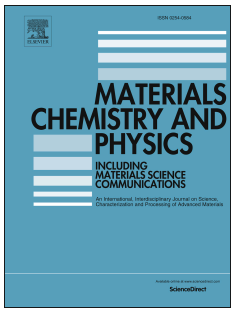

Pressure Assisted Bonding Process of Stainless Steel on Titanium Alloy Using Powder Metallurgy

Fuad Khoshnaw, Ridvan Yamanoglu, Umit Gencay Basci, Onur Muratal

PII: S0254-0584(20)31375-4

DOI: https://doi.org/10.1016/j.matchemphys.2020.124015

Reference: MAC 124015

To appear in: *Materials Chemistry and Physics*

Received Date: 22 April 2020

Revised Date: 27 August 2020

Accepted Date: 3 November 2020

Please cite this article as: F. Khoshnaw, R. Yamanoglu, U.G. Basci, O. Muratal, Pressure Assisted Bonding Process of Stainless Steel on Titanium Alloy Using Powder Metallurgy, *Materials Chemistry and Physics*, https://doi.org/10.1016/j.matchemphys.2020.124015.

A new approach to joint stainless steel and titanium alloys by powder metallurgy was succesfully desgined.

A strong interface layer was obtained without adding interlayer elements.

Titanium alloy bonded with stainless steel showed enhanced wear resistance.

Increasing the temperature caused formation of the larger interface thickness.

Large interface thickness caused less strength, high brittleness, and easily debonding.

Pressure Assisted Bonding Process of Stainless Steel on Titanium Alloy Using Powder Metallurgy

Fuad Khoshnaw[1], Ridvan Yamanoglu[2], Umit Gencay Basci[2], Onur Muratal[2]

[1]School of Engineering and Sustainable Development, De Montfort University, Leicester, United Kingdom
fuad.hassankhoshnaw@dmu.ac.uk

[2]Metallurgical and Materials Engineering Department, Kocaeli University, Kocaeli, Turkey
ryamanoglu@kocaeli.edu.tr, onurmuratal@gmail.com

Abstract

Titanium alloys have been widely used in many industrial applications. Nevertheless, efforts to improve their properties are continually increasing. One of the most effective routes to improve strength, hardness and wear resistance is to create a coating layer on the substrates. In the current study, stainless steel was selected for the in-situ joining and creating a continuous layer on the Ti6Al4V alloy. The Joining process was carried out at two different temperatures, 950 ^{o}C and 1050 ^{o}C, and the mechanical properties of the bonded materials were investigated employing hardness, bending strength and wear tests, while the bonding interface layer between the alloys powders was characterized by optical and scanning electron microscopes. The results showed that the higher the joining temperature, the wider the interfacial zone between the coating layer and substrate. The hardness and wear properties of the joint materials increased at 1050^{o}C, while the bending stress was reduced and debonding was observed after the bending test. The chemical composition at the interface zone was identified by energy dispersive X-ray analysis, and the results showed high diffusion rates between the elements. As a result, the process used in the current study can be used for many titanium alloys, and their use in industrial applications can be increased.

Keywords: Ti6Al4V, stainless steel, dissimilar joints, powder metallurgy, interface

Corresponding author: Ph.D. Ridvan YAMANOGLU; Tel: +90 262 303 3060, Fax: +90 262 303 3003

E-mail address: ryamanoglu@kocaeli.edu.tr

Introduction

Recently, due to the requirement of high-performance materials for many industrial applications, the joining of dissimilar materials have attracted many researchers. When considering dissimilar metallic materials, titanium and stainless steel alloys are preferred in various engineering fields because of their excellent corrosion resistance, high mechanical properties and excellent biocompatibilities. Therefore, joining these two metallic materials can provide enhanced mechanical and physical properties [1]. However, different brittle phases occur at the interface between stainless steel and titanium alloys are obtained by the joining processes which need relatively high temperatures. These brittle intermetallic phases can result in lowering the fracture toughness and corrosion resistance. The reason for the formation of these brittle intermetallic compounds can be explained through analyzing equilibrium phase diagrams. For example, the solubility of Fe in Ti is 0.1 %, at room temperature. Above this ratio, brittle intermetallic phases of Ti_xFe_y, Ti_xNi_y, and Ti_xCr_y are formed. Subsequently, this leads to cracks under loading conditions [1-4]. When it comes to austenitic stainless steel alloys, Khoshnaw [5] indicated that they are exposed to the formation of brittle phases and carbide precipitation, e.g. Cr_xC_y when they pass through sensitization ranges between 550^{o}C and 850^{o}C.

Many joining techniques, such as welding, brazing and diffusion bonding, are applied to Ti and stainless steel alloys [6-8]. Within these techniques, solid-state techniques are generally preferred compared to fusion-based, due to the differences in their physical properties, such as thermal expansion coefficient: Ti equals 8.9 x 10^{-6} $^{o}C^{-1}$ and Fe equals 12.2 x 10^{-6} $^{o}C^{-1}$, the melting point for Ti equals 1660 ^{o}C and for Fe is 1532 ^{o}C. Bonding of different materials is restricted by different factors such as their large difference in physical properties and melting points. Those differences cause some residual stress trapped at the interface of the bonding zone. The most commonly used solid-state technique is diffusion bonding, as this enables a reduction in several melting-based interface problems [9]. Examples of solid-state joining are friction welding and diffusion bonding used to join titanium and stainless steel to avoid interfacial melting at the interface. Dey *et al*. found that better tensile strengths are obtained in the Ti base material utilizing friction welding [10].

Titanium alloy type Ti6Al4V, which covers about half of the total world production of titanium alloys, is preferred for many engineering applications such as those used in the military, automotive, aerospace, marine, and medical industries, due to their high specific strength, corrosion resistance, low cost to performance ratio and biocompatibilities. However,

the poor tribological properties of Ti6Al4V alloy limit its successful implementation in the intended applications [11]. The reason for the poor wear resistance is tribooxides which are very brittle and do not adhere to the surface. These tribooxide layers are easily removed from the surface during sliding conditions. Low plastic share characteristics and surface energy are the other aspects of negative factors on low wear resistance of titanium alloys [12-13]. In terms of bonding of powder alloys, the conventional powder metallurgy techniques cause a coarse microstructure with low mechanical properties. At the same time, the hot pressing technique provides high density, reducing the adverse effects of initial powder shape and size characteristics and controlling the interface thickness [14]. Pressure assisted techniques also provide a direct benefit to the densification and final properties of the material. Applied pressure during sintering has been found to enhance the densification rate and reducing sintering temperature and holding time, resulting in improved mechanical properties [15].

Many researchers are trying to develop new processes to enhance the final properties of titanium alloys. One of the essential properties of the titanium-based materials is their corrosion behaviour. We aimed to combine stainless steel and Ti6Al4V alloy, and designed a new bonding process to develop improved tribological properties. This new route represents a solid-state bonding process between Ti6Al4V and 316L stainless steel powder alloys using a powder metallurgical hot-pressing technique. This approach is novel because of the combination of these two different powder alloys, without adding interlayer elements, and provides enhanced performance.

Materials and Experimental Works

Characterization of the Powder Alloys

The preliminary materials used in this study were hydride-dehydride HDH Ti6Al4V powders: 6.2Al, 4.14V, 0.02Si, 0.14Fe, bal. Ti (wt.%) and water atomized stainless steel: 17.6Cr, 13.6Ni, 2.9Mo, 2.0Mn, 1.2Si, 0.03C, bal. Fe (wt.%) powders. Figure 1a and 1b show the scanning electron microscopy - SEM images of the Ti6Al4V and stainless steel particles, respectively. The shape of the Ti6Al4V alloy powders is irregular, and the size of the particles is < 150 μm while the shape of the stainless steel powder is approximately circular shape with size ranges of 50-100 μm. The shape of the particles strongly depends on the production method. For example, titanium particles are made brittle because their exposure to hydrogen; the brittle particles are milled and finally are heat-treated under a vacuum atmosphere to remove hydrogen. As a result, the mechanical milling produces irregular shape particles.

Meanwhile, stainless steel powders are produced by water atomization. As the liquid metal is broken apart by water, usually round shape particles are produced due to the fast cooling of the liquid metal with the interaction of water. Subsequently, particles with round or semi-round shapes are produced [16]. The hot pressing technique - used in this study - eliminates the irregular shape effect of the particles on the low density of the product. The particles can deform under pressure easily, and the density increases with an activated neck bonding mechanism between the particles [15].

Bonding Process

In this study, a hot compaction diffusion bonding mechanism through applying uniaxial hot-pressing technique was used. To perform the bonding process of coating 300 μm stainless steel powder alloy type 316L on Ti6Al4V power alloy was performed. No interlayer material used. Figure 2 shows the schematic illustration of the hot press process. The thickness of the desired material layer can be controlled by adding known amounts of the powder. The figure shows that loose Ti6Al4V powders were placed firstly inside the graphite die; then stainless steel powders were poured onto the titanium powders to form a layer of thickness 300 μm. A 0.2 mm graphite paper was added for lubrication and to facilitate the release of the bonding compacts from the mould body after hot pressing. Two graphite punches with an outer diameter of 20 mm were inserted into the graphite die body and faced with graphite foil to supply a uniform contact resistance between die and punches.

The process was carried out using a DIEX brand (Korea) hot press. The dimensions of the final compacts were 20 mm diameter and 5 mm thickness, both stainless and Ti layers. Two different in-situ coating bonding temperatures, 950^{o}C and 1050^{o}C, were applied during the process. The holding time at both temperatures was kept constant as 30 minutes under 50 MPa. The details of the process cycle are shown in Figure 3. The whole bonding process was carried out under vacuum to prevent oxidation.

Metallographic Preparation and Mechanical Tests

The combined materials were metallographically prepared for microstructural characterization and mechanical tests. Ground papers 320, 600, 1000 and 2000 grits were used for grinding, and 9, 6, 3 and 1 μm diamond suspensions were used for polishing. For consistency, 2 minutes duration was kept constant for each polishing process. The samples were etched by Kroll reagent for 10 seconds based on ASTM 192. The density of the bonded compacts was measured at room temperature by using Archimedes' principle, according to ASTM Standard

B962-08. The microstructure of the samples with etched surfaces was examined using an electron microscope. SEM images and EDX investigations were carried out using Jeol 6060. The hardness of the samples was measured using a Vickers hardness test by applying 10 kg. The bending behaviour of the samples was determined by INSTRON Model 300LXJ. The tribological performance of the bonded materials was carried out by a Nanovea MT/60/NI-type ball on disc tribometer, which was used to measure the friction coefficient. The dry sliding wear behaviour of the produced samples was determined at room temperature under 15 N. The sliding speed and sliding distance were 0.06 ms^{-1} and 250 m, respectively. An alumina ball with 6 mm diameter was used as the counterface. The samples were cleaned with alcohol after the wear tests, then dried with a hot air blower. The following formula was used to calculate the wear rate of the samples [17]:

$$W=M/\rho D$$

where W is the wear rate ($mm^3.m^{-1}$), M denotes mass loss (g), ρ ($g.mm^{-3}$) and D (m) are the density and sliding distance, respectively.

Results and Discussion

Table 1 shows the relative densities as a function of bonding temperatures. The temperature is the most effective sintering parameter on the diffusion between particles, resulting in higher densities. The bonded sample sintered at 950 ^oC had a density of 96,4%, while the sample bonded at 1050 ^oC had a density of 99,8% showing almost a full density. In general, the results showed that the density of the bonded materials increased with the increasing sintering temperature.

Microstructural Characterization

Figure 4 shows the bonded coating thickness of stainless steel on Ti6Al4V alloy, as in average equals 300 μm, which shows relatively high homogeneity of the stainless steel layer. This homogeneousness is an important property for the coated material because the interlayer between bonded materials is strongly affecting the final properties of the materials. Thick coating materials and techniques are necessary for tribological and load-bearing applications. Formation of a weak bond zone results in a reduction in the tensile strength and toughness properties of the interlayer. Subsequently, cracks and delamination are possible at the interface and this decreases the service life [18].

Figure 5a and b show the interface thickness as a function of production temperatures at 950 ^{o}C and 1050 ^{o}C, respectively. The diffusion layer increased with increasing temperature. The thickness of the interface layers was equal to approximately 100 μm and 150 μm for 950 ^{o}C and 1050 ^{o}C, respectively.

To investigate the interface layers at 1050 ^{o}C, four zones, numbered as 1, 2, 3 and 4 were selected within the stainless steel and titanium alloy interface layer. In each zone, three points, named A, B and C were chosen to be analyzed by EDX, except zone 2, where only 2 points were chosen (see Figure 6). Table 2 shows a quantitative elemental analysis of the points as a weight percentage.

Zone 1 is the stainless steel side of the bonding materials. Three different points were analyzed. Table 2 shows that zone 1 is characterized by standard stainless steel elements. However, some small amount of the Ti, Al and V elements were also observed in zone 1. Point B is shown as a dark grey thin lamellar between stainless steel and the interface. Titanium and aluminium elements diffused towards the stainless steel zone and produced this thin zone. The remaining Ti and Al caused different types of phase with Fe, Cr, and Ni elements are given in Table 2. The main reason for the different layers with different elements is the variation of diffusion rates of the elements in the material. In particular, Fe and Ni diffuse fast and migrate inside the titanium easily, which causes different compounds at the interfaces, as shown in Figure 6, Zone 1, point B [19]. As a result, a layer of material containing different amounts of titanium and iron with different depth of diffusion layers occurs. Different diffusion rates of Ti and Fe within each other produce intermetallic Ti_xFe_y compounds with an irregular geometric shape as shown in Figure 6, zone 1, point C [20].

Zone 2 microstructure belongs to Ti6Al4V alloy size of the bonding materials. Ti6Al4V alloy has α+β structure showing an equiaxed shape hexagonal close-packed α grains and β phases distributed around the body-centred cubic α grains. Light lamellar areas of vanadium rich zoned of β phase is shown, while dark equiaxed grains are α rich zones. This approach was proved through the chemical analysis of zone 2, points A and B, as shown in Table 2. The chemical composition of the α and β phase are relatively different, as the α phase consists of less V than β, while the later phase consists of both Al and V elements. Similar results were found by Siqueira *et al.* [21], and they explained the solubility of the β stabilizing element in the α phase at room temperature. Therefore, β stabilizing elements in a phase could not be

detected [21-22]. The chemical composition of zone 2 was changed towards the interface layer, and new phases with different geometric shapes were observed.

For zones 3 and 4, which are symmetrical across the interface layer, Table 2 shows that elements, especially Fe, Cr and Ni were identified by EDX as shown in Table 2. Point C in zone 3 is the closest region of the interface to the Ti6Al4V side. Therefore, the chemical composition was not changed very much and remained similar to zone 2, point A. The solubility of Fe, Cr and, Ni in the phase is limited, and their amount is relatively low. The structure of point B is similar to point C. However, the composition is different. The content of V element of this zone was found lower compared to point C and, unlike Fe content, Cr and Ni content of this phase were found to be high. The chemical composition of point A in zone 3 consisted of a high amount of Fe, Cr and Ni elements beside the Ti, al and V. This composition is seen as a base interface zone consisting of all the bonded elements. In this zone, the difference in the diffusion capabilities of the elements caused a formation of new phases, as shown in zone 4 (see Figure 6). In addition to that, the effect of the shape and size of the selected points was investigated by EDX. Large grains with sharp edges consisted of mainly Ti and Fe elements. These phases also contained a high amount of Ni, Cr, Al and V. Unlike point A in zone 3, the point B in zone 4 contains high amounts of Fe, Cr and Ni instead of Al and V. This is an expected result due to being close to the stainless steel side in the bonded interface layer. These large phases transformed finely distributed constituents containing mainly Fe, Ni, Al, Cr and V.

Hardness Test

Figure 7a (bonded at 950 ^{o}C) and 7b (bonded at 1050 ^{o}C) show the hardness values of the bonded materials across their cross-sectional areas started at 75 microns depth. The bonded materials showed a different hardness profile as a function of bonding temperatures at 950 ^{o}C and 1050 ^{o}C. The hardness values of the three layers; stainless steel as a surface material, Ti6Al4V as a substrate and the interface layer, were increased by increasing the applied temperature. The high hardness of surface and substrate can be attributed to the enhanced density due to the increasing consolidation of stainless steel and titanium alloy particles at high temperature. The hardness of surface - stainless steel - and substrate – titanium alloy - of the bonded material increased from about 200 to 300 HV, and from 350 to 450 HV, respectively. Moreover, the interface hardness was also increased extensively with increasing temperature; the hardness of the interface layer reached up to 700 HV and 1150 HV at 950 ^{o}C and 1050 ^{o}C, respectively. A sharp increase in the hardness was observed at the bonded

interface close to the stainless steel side, and the hardness from the pick value decreased gradually through the titanium alloy side. High hardness increase at the interface is due to the formation of different intermetallics. Ti, Al, and V from substrate and Fe, C, Mn, Ni, Cr, and Si from coating layer can cause a formation of TiC, Al_2Fe, Al_3Ti, AlTi, Fe_2V_3, Mn_2Ti, $Fe_3Al_2Si_4$, Al_6Ti_{19}, NiTi, Ni_3Ti, $NiTi_2$, Ni_2Ti compounds. Besides, C atoms can diffuse along with the interface and form $(Fe, Cr)_3C$ phase [23].

Bending Test

A three-point bending test was selected to determine the mechanical properties of the bonded samples. Figure 8 shows the three-point bending test results of the diffusion bonded samples. The bending strength decreased with increasing bonding temperature. The bonded material produced at 950 ^oC has a higher bending strength equal to 1332 MPa while the bonded materials produced at 1050 ^oC exhibited a bending strength of 1261 MPa. Similarly, the displacement values of the bonded materials decreased with the increase of the temperature from 950 ^oC (1.33 mm) to 1050 ^oC (1.05). Figure 9 shows SEM images of the failed samples after the bending tests, and Figure 9b shows large debonding within the interface layer formed at 1050 ^oC This result can be attributed to the thickness of the interface between the bonded materials at different temperatures, as the results showed that the interface layer formed at 1050^oC exhibited a considerably larger thickness compared to the sample produced at 950 ^oC. This can be attributed to the large interface layer associated with different high hardness phases, which could not sustain the bending stress. So the material failed [24].

The different intermetallic compounds occurring at the interface has mainly a brittle nature. High hardness of the phases at the interface and increasing interlayer thickness tend to decrease the plasticity of the bonded layer and decrease the quality of the joints [25]. On the other hand, this phenomenon can be illustrated based on the non-uniform distribution of the Von Mises stresses which occur with the increase of thickness of the bonded interface, causing a decrease of the shear strength. When the temperature increases the thickness of the interface and different intermetallic formed, this caused a decrease in the shear strength. Overloading conditions easily cause failures at the interface for those reasons [26].

Figure 10 shows the SEM fractography images of the cross-sectional areas of the bonded samples, broken after the bending test. A low magnification image of the stainless steel surface shows an interparticle fracture mechanism, also, large cracks between stainless steel particles are seen. The reason behind that can be attributed to the temperature bonding of the

stainless steel particles at 950 ^{o}C, which was not enough to enhance the diffusion process. On the other hand, since stainless steel particles were produced by water atomization, this type of powder forms a surface oxide layer that adheres the diffusion of the elements that causes low density, consequently fracture occurs along the particle's surfaces [27]. The fractography image of the stainless steel layer produced at 1050 ^{o}C showed ductile fracture with small and elongated dimples. Dark and flat surfaces indicate the brittle fracture surfaces. Bright areas show typical fracture characteristics of ductile materials with small dimples. Unlike the stainless steel side produced at 950 ^{o}C, no interparticle fracture defects were observed on the fracture surface of the stainless steel side bonded at 1050^{o}C. Both the titanium side bonded at 950 ^{o}C and 1050 ^{o}C exhibited mainly ductile fracture with elongated dimples. However, with the increasing of bonding temperature, ductile fracture mode increases. Ti6Al4V produced at 950 ^{o}C showed some large cleavage surfaces indicating brittle fracture failure.

Wear Test

Although titanium and its alloys have superior physical and mechanical properties, their wear properties restrict their usage in many industrial applications. Dry sliding wear properties of bonded stainless steel and Ti6Al4V alloy were investigated. Table 3 shows the wear rate results of the bonded materials produced at two different temperatures. The results show that the bonding of titanium alloy with stainless steel caused an intensive increase in the wear resistance. The wear rate of the Ti6Al4V alloy produced at 950 ^{o}C was 10.20, while Ti6Al4V alloy bonded with stainless steel resulted in the wear rate decreasing to 4,87 $mm^{3}m^{-1}10^{-3}$. Similarly, the wear rate of the Ti6Al4V alloy produced at 1050 ^{o}C showed a wear rate equal to 8,37 $mm^{3}m^{-1}10^{-3}$. However, when the Ti6Al4V alloy bonded with stainless steel at 1050 ^{o}C, the wear rate decreased to 1,62 $mm^{3}m^{-1}10^{-3}$.

Figure 11 shows the friction coefficient of Ti6Al4V as a substrate, with and without coating stainless steel powder, at both temperatures. The results show that the friction coefficient for both types of samples, with and without coating, decreased with increasing temperature. The friction coefficient factor decreased from 0.6 to 0.55 and from 0.4 to 0.35 for coated stainless steel and Ti6Al4V substrate, respectively. High temperatures provide higher densification during the sintering process resulting in lower friction coefficient for both titanium and stainless steel [28].

Although the friction coefficient of Ti6Al4V alloy is lower than that of stainless steel bonded material, the wear rate of the stainless steel bonded material is relatively lower than Ti6Al4V

substrate (see Table 3). The reason behind that can be attributed to the oxide layer on Ti6Al4V as it is more stable and decreases the friction coefficient; however, the oxide layer on titanium surface can be easily removed from the surface during the dry sliding wear condition resulting in higher wear rate.

SEM images of worn surfaces of both materials have a good correlation with the wear rate results as shown in Table 3. As expected, the worn surface of the Ti6Al4V shows higher materials removed from the surfaces compared to the stainless surface for both bonding temperatures. Figure 12 shows the SEM images of worn surfaces for stainless steel and Ti6Al4V alloy surfaces at both 950 ^{o}C and 1050 ^{o}C. The results indicate that stainless steel shows a smoother surface compared with the Ti6Al4V alloy surface. The stainless steel surface obtained at 950 ^{o}C showed mainly abrasive wear with narrow grooves, and some surface cracks can be seen due to the low density of the bonded material. However, when the bonding temperature increased to 1050 ^{o}C no visible crack on the surface is seen. It is clear from the surface that with the increase of temperature, the wear mechanism is the combination of abrasion and adhesion on the stainless steel surface. High plastic deformation with the proof of large deformed grooves showing a ploughing mechanism on the Ti6Al4V surface at 950 ^{o}C is seen in Figure 12). When the temperature increased to 1050 ^{o}C, no large grooves on Ti6Al4V surface are seen, and a mainly smooth worn surface is observed. In the middle of Figure 12d, rupture of some oxide zones from the surface is clearly seen. By means of a decreasing amount of high plastic deformation, less material loss occurred on the surface and the wear rate of the Ti6Al4V alloy increased with increasing temperature from 950 to 1050 ^{o}C. As a result, both materials showed better wear characteristics with increasing temperature. This can be correlated to the higher hardness and density of the materials.

Conclusions

In the current study, a new approach was developed for the enhanced properties of titanium-based materials. For this purpose, stainless steel powders were *in situ* coated on Ti6Al4V alloy by powder metallurgical methods under pressure conditions. The results showed that this new process can be used different titanium alloys, and their use in many industrial applications can be increased. Following conclusions were obtained:

- Assisting pressure during the bonding process enhanced the diffusion behaviour of the elements and increased the density of the whole material with a strong bonding

interface layer. The strong bonding of the substrate and coating layer is vital, especially for load-bearing applications.

- Titanium-based materials show weak wear resistance. Significant improvement has been achieved in wear resistance with the coating of stainless steel. When the Ti6Al4V alloy bonded with stainless steel at 1050 ^{o}C, the wear rate decreased from 8,37 to 1,62 $mm^3m^{-1}10^{-3}$.
- Higher temperatures enhance the densification resulting in improved wear resistance. The wear rate of the bonded sample at 1050 ^{o}C was lower than the wear rate at 950 ^{o}C, as expected.
- However, higher temperature produced the formation of a larger interface thickness caused less strength, high brittleness, and easy debonding.

Acknowledgement

This study is funded by De Montfort University in the United Kingdom as part of the internal Further Funding VC2020 scheme. Accordingly, a shared research project was conducted in January 2019 with Kocaeli University (Supported by Scientific Research Project Unit, Project Number: 2018/158) in Turkey.

References

[1]. J. Lee, M. Lee, Microstructure and mechanical behavior of a titanium to stainless steel dissimilar joint brazed with Ag-Cu alloy filler and an Ag interlayer, Materials Characterization, 129 (2017) 98-103.

[2] S. Chen, M. Zhang, J. Huang, C. Cui, H. Zhang, X. Zhao, Microstructure and mechanical property of laser butt welding of titanium alloy to stainless steel, Materials and Design, 53 (2014) 504-511.

[3] A. Mirijev, A. Stern, E. Tuval, S. Kalabukhov, Z. Hooper, N. Frage, Titanium to steel joining by spark plasma sintering (SPS) technology, Journal of Materials Processing Technology, 213 (2013) 161-166.

[4] Y. Zhang, D. Sun, X. Gu, H. Li, A hybrid joint based on two kinds of bonding mechanisms for titanium alloy and stainless steel by pulsed laser welding, Materials Letters, 185 (2016) 152-155.

[5] F. Khoshnaw and R. Gardi, Sensitization assessment of duplex stainless steel using critical pitting temperature CPT method - ASTM G48, Buletnul Instititutului Politechnic Din Iasi, 3 (2007) 261-268.

[6] I. Tomashchuk, D. Grevey, P. Sallamand, Dissimilar laser welding of AISI 316L stainless steel to Ti6-Al4V alloy via pure vanadium interlayer, Materials Science and Engineering A, 622 (2015) 37-45.

[7] Y. Xia, P. Li, X. Hao, H. Dong, Interfacial microstructure and mechanical property of TC4 titanium alloy/316L stainless steel joint brazed with Ti-Zr-Cu-Ni-V amorphous filler metal, Journal of Manufacturing Processes, 35 (2018) 382-395.

[8] D. Yongqiang, S. Guangmin, Y. Lijing, Impulse pressuring diffusion bonding of titanium to stainless steel using a copper interlayer, Rare Metal Materials and Engineering 44(5) (2015) 1041-1045.

[9] P. Li, J. Li, M. Salman, L. Liang, J. Xiong, F. Zhang, Effect of friction time on mechanical and metallurgical properties of continuous drive friction welded Ti6Al4V7SUS321 joints, Materials and Design, 56 (2014) 649-656.

[10] H. C. Dey, M. Ashfaq, A. K. Bhaduri, K. Prasad Rao, Joining of titanium to 304L stainless steel by friction welding, Journal of Materials Processing Technology, 209 (2009) 5862-5870.

[11] D. Kumar, K. B. Deepak, S. M. Muzakkir, M. F. Wani, K. P. Lijesh, Enhancing tribological performance of Ti-6Al-4V by sliding process, Tribology-Materials, Surfaces & Interfaces, (2018) 1-7.

[12] G.D. Revankar, R. Shetty, S.S. Rao, V.N. Gaitonde, Wear resistance enhancement of titanium alloy (Ti–6Al–4V) by ball burnishing process, Journal of Materials Research and Technology 6(1) (2017) 13-32.

[13] Y. Zi-Run, H. Hai-Xiang, C.-F. Jiang, W.-M. Li, X.-R. Liu, S. Lyu, Evaluation on dry sliding wear behavior of (TiB+TiC)/Ti-6Al-4V matrix composite, International Journal of Precision Engineering and Manufacturing 18(8) (2017) 1139-1146.

[14] M. Hasan, J. Zhao, Z. Huang, L. Chang, H. Zhou, Z. Jiang, Analysis of sintering and bonding of ultrafine WC powder and stainless steel by hot compaction diffusion bonding, Fusion Engineering and Design, 133 (2018) 39-50.

[15] R. Yamanoglu, Pressureless spark plasma sintering: A perspective from conventional sintering to accelerated sintering without pressure, Powder Metallurgy and Metal Ceramics, 57 (2019) 513-525.

[16] L. Bolzoni, E. Herraiz, E. M. Ruiz-Navas, E. Gordo, Study of the properties of low-cost powder metallurgy titanium alloys by 430 stainless steel addition, Materials & Design, 60 (2014) 628-636.

[17] R. Yamanoglu, Production and characterization of Al-xNi In situ Composites Using Hot Pressing, Journal of Mining and Metallurgy Sect. B., 50(1) B (2014) 45-52.

[18] K. Holmberg, A. Matthews, Tribology of engineered surfaces, in Wear, Materials, Mechanisms and Practice, ed. by G.W. Stachowiak (John Wiley & Sons Ltd, Chichester, 2006), pp. 123–166.

[19] H. Mishra, D. V. V. Satyanarayana, T. K. Nandy, P. K. Sagar, Effect of trace impurities on the creep behavior of a near a titanium alloy, Scripta Materialia, 59 (2008) 591-594.

[20] V. P. Shapovalov, A. N. Kurasov, Diffusion of titanium in iron, Metal Science and Heat Treatment, 17 (9) (1975) 803-805.

[21] R. P. Siqueira, H. R. Z. Sandim, A. O. F. Hayama, V. A. R. Henriques, Microstructural evaluation during sintering of blended elemental Ti-5Al-2.5Fe alloy, Journal of alloy and compounds, 476 (2009) 130-137.

[22] A. Y. Fasasi, S. Mwenifumbu, N. Rahbar, J. Chen, M. Li, A. C. Beye, C. B. Arnold, W. O. Soboyejo, Materials Science and Engineering C, 29 (2009) 5-13.

[23] D. F. Mo, T.F. Song, Y. J. Fang, X. S. Jiang, C. Q. Luo, M. D. Simpson, Z. P. Luo, A review on diffusion bonding between titanium alloys and stainless steels, Advances in Materials Science and Engineering, 2018 (2018) 1-15.

[24] M. Saboktakin, G. R. Razavi, H. Monajati, The investigate metallurgical properties of roll bonding titanium clad steel, International Journal of Applied Physics and Mathematics, 1(3) (2011) 177-180.

[25] T. F. Song, X. S. Jiang, Z. Y. Shao, Y. J. Fang, D. F. Mo, d. G. Zhu, M. H. Zhu, Microstructure and mechanical properties of diffusion bonded joints between Ti-6Al-4V titanium alloy and AISI316L stainless steel using Cu/Nb multi-interlayer, Vacuum, 145 (2017) 68-76.

[26] A. A. M. Elrefaey, W. Tillmann, , Microstructure and mechanical properties of brazed titanium7steel joints, Journal of Materials Science, 42(23) (2007) 9553-9558.

[27] Y. Zhang, E. Feng, W. Mo, Y. Lv, R. Ma, S. Ye, X. Wang, P. Yu, On the microstructures and fatigue behaviors of 316L stainless steel metal injection molded with gas-and-water atomized powders, Metals, 8(893) 2018 1-13.

[28] M. Fellah, N. Hezil, K. Abderrahim, M. A. Samad, A. Montagne, A. Mejias, S. Weiss, Investigating the Effect of Sintering Temperature on Structural and Tribological Properties of a Nanostructured Ti–20Nb–13Zr Alloy for Biomedical Applications. In Characterization of Minerals, Metals, and Materials, (2020) 619-629.

FIGURE CAPTIONS

Figure 1. SEM images, a- Ti6Al4V powder, b - stainless steel powder

Figure 2. Schematic illustration of hot-pressing process for stainless steel and Ti6Al4V alloy

Figure 3. In-situ bonding and thermal cycle during bonding of stainless steel and Ti6Al4V alloy at two different temperatures

Figure 4. Optical image of bonding of stainless steel as a coating layer on Ti6Al4V alloy

Figure 5. Interface layer of bonded materials at a) 950 ^{o}C and b) 1050 ^{o}C

Figure 6. SEM images of EDX analyzed zones at the bonded interface at 1050^{o}C bonding process

Figure 7. Hardness values of the bonded materials as a function of joining temperature, a) 950 ^{o}C, and b) 1050 ^{o}C.

Figure 8. Bending test result of the bonded materials produced at 950 and 1050 ^{o}C

Figure 9. Fracture surface of bonded material at different temperatures; a) 950 ^{o}C, b) 1050 ^{o}C

Figure 10. Fracture surface of stainless steel and Ti6Al4V alloy, a) stainless steel at 950 ^{o}C, b) stainless steel at 1050 ^{o}C, c) Ti6Al4V at 950 ^{o}C, and d) Ti6Al4V at 1050 ^{o}C.

Figure 11. Friction coefficient of stainless steel and Ti6Al4V alloy for different bonding temperatures, a) 950 ^{o}C, b) 1050 ^{o}C

Figure 12. SEM images of worn surfaces, a) Stainless steel at 950 ^{o}C, b) Stainless steel at 1050 ^{o}C, c) Ti6Al4V at 950 ^{o}C, d) Ti6Al4V at 1050 ^{o}C

TABLE CAPTIONS

Table 1. Density of produced samples at two different sintering temperatures

Table 2. Chemical composition of the interface layer at 1050^{o}C bonding process

Table 3. Wear rates of bonded materials as a function of temperature

Pressure Assisted Bonding Process of Stainless Steel on Titanium Alloy Using Powder Metallurgy

Abstract

Titanium alloys have been widely used in many industrial applications. Nevertheless, efforts to improve their properties are continually increasing. One of the most effective routes to improve strength, hardness and wear resistance is to create a coating layer on the substrates. In the current study, stainless steel was selected for the in-situ joining and creating a continuous layer on the Ti6Al4V alloy. The Joining process was carried out at two different temperatures, 950 ^{o}C and 1050 ^{o}C, and the mechanical properties of the bonded materials were investigated employing hardness, bending strength and wear tests, while the bonding interface layer between the alloys powders was characterized by optical and scanning electron microscopes. The results showed that the higher the joining temperature, the wider the interfacial zone between the coating layer and substrate. The hardness and wear properties of the joint materials increased at 1050^{o}C, while the bending stress was reduced and debonding was observed after the bending test. The chemical composition at the interface zone was identified by energy dispersive X-ray analysis, and the results showed high diffusion rates between the elements. As a result, the process used in the current study can be used for many titanium alloys, and their use in industrial applications can be increased.

Keywords: Ti6Al4V, stainless steel, dissimilar joints, powder metallurgy, interface

Table 1. Density of produced samples at two different sintering temperatures

Materials	Relative density (%)
Ti6Al4V-coated with 316L SS at 950 ^{o}C	96,4
Ti6Al4V-coated with 316L SS at 1050 ^{o}C	99,8

Table 2. Chemical composition of the interface layer at 1050^{o}C bonding process

	Composition (wt.%)						
Zone	Point	Ti	Al	V	Fe	Cr	Ni
1	A	0,186	0,058	0,283	69,672	16,653	13,148
	B	97,039	0,310	---	1,598	0,356	0,6970
	C	65,659	1,754	0,295	17,818	2,028	12,446
2	A	91,105	7,235	1,660	---	---	---
	B	86,901	6,418	6,681	---	---	---
3	A	76,892	7,375	3,793	8,898	1,096	1,946
	B	91,205	6,534	0,741	0,372	0,443	0,705
	C	90,341	7,283	1,302	0,565	0,243	0,266
4	A	52,740	4,229	1,302	30,608	4,303	6,818
	B	68,236	5,758	2,283	15,888	4,500	3,335
	C	84,283	2,188	0,465	8,034	1,504	3,526

Table 3 Wear rates of bonded materials as a function of temperature

Material	Wear rate (mm^3/m)x10^{-3}
Ti6Al4V as substrate at 950 ^oC	10,20
Ti6Al4V as substrate at 1050 ^oC	8,37
316L SS bonded on Ti6Al4V at 950 ^oC	4,87
316L SS bonded on Ti6Al4V at 1050 ^oC	1,65

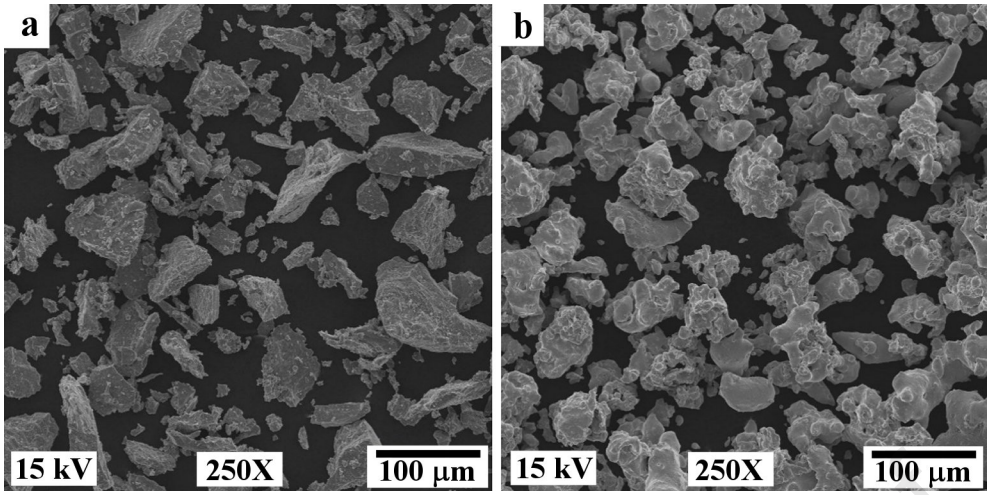

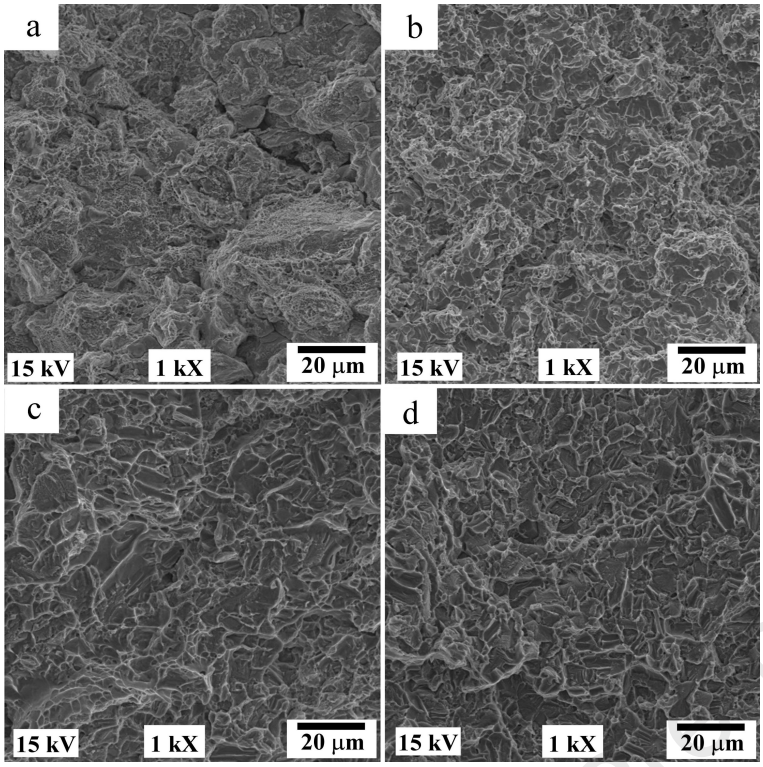

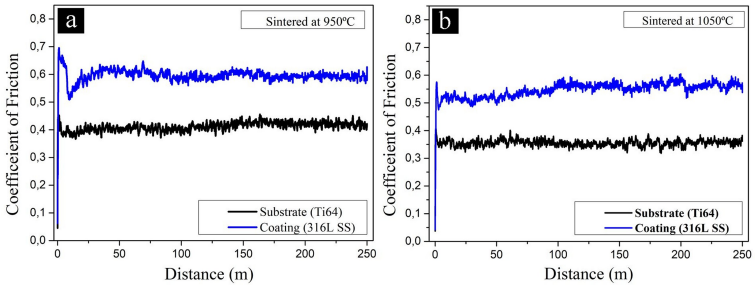

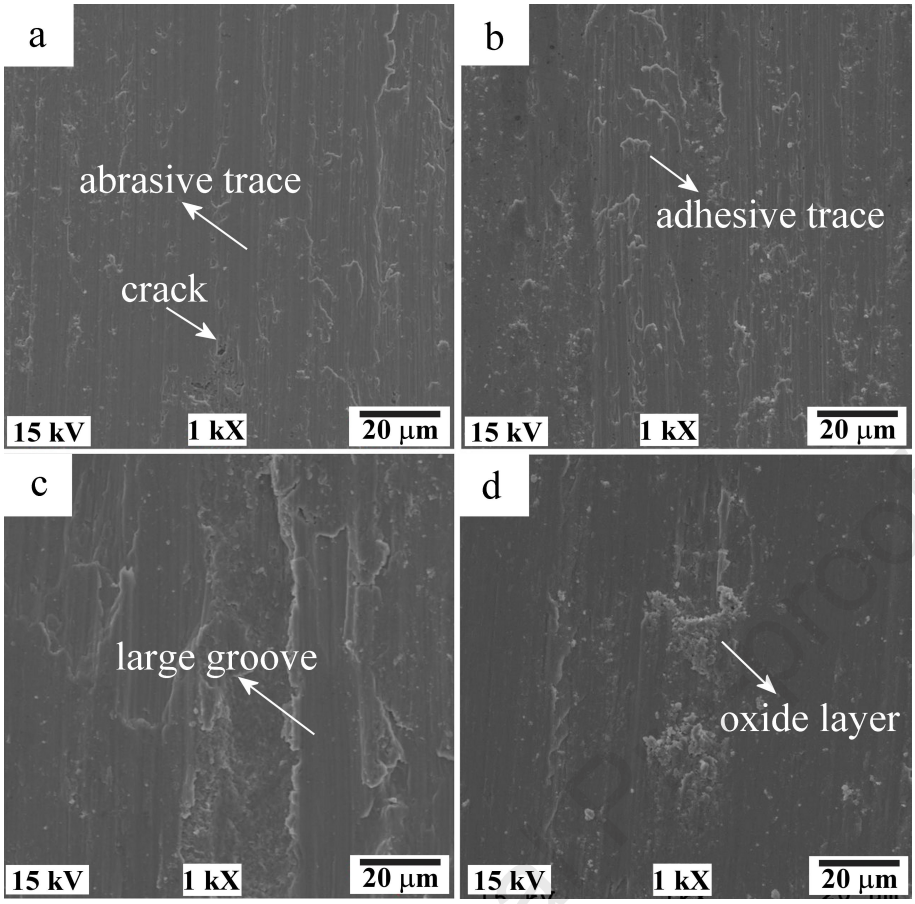

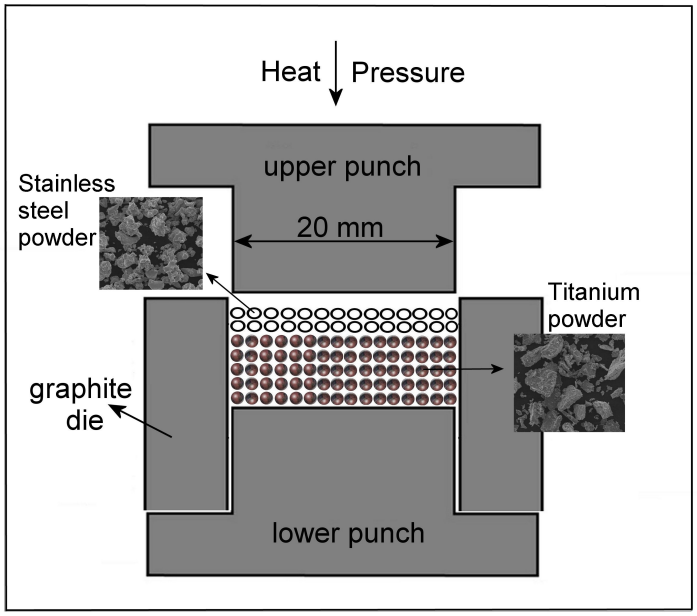

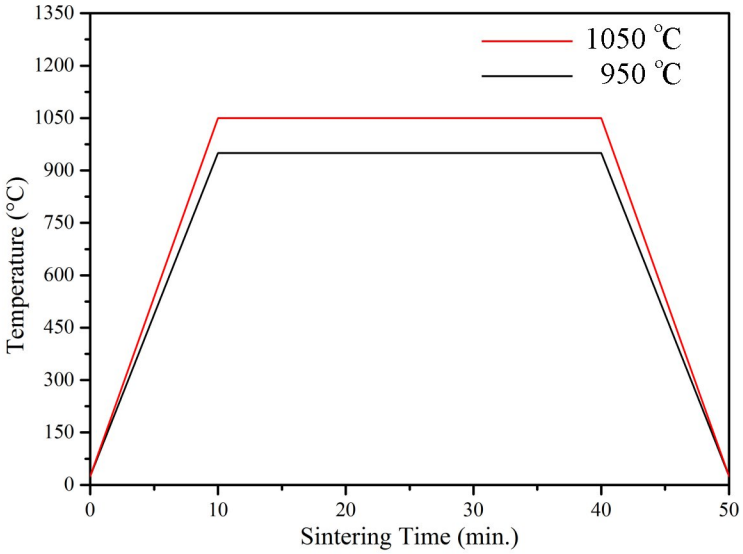

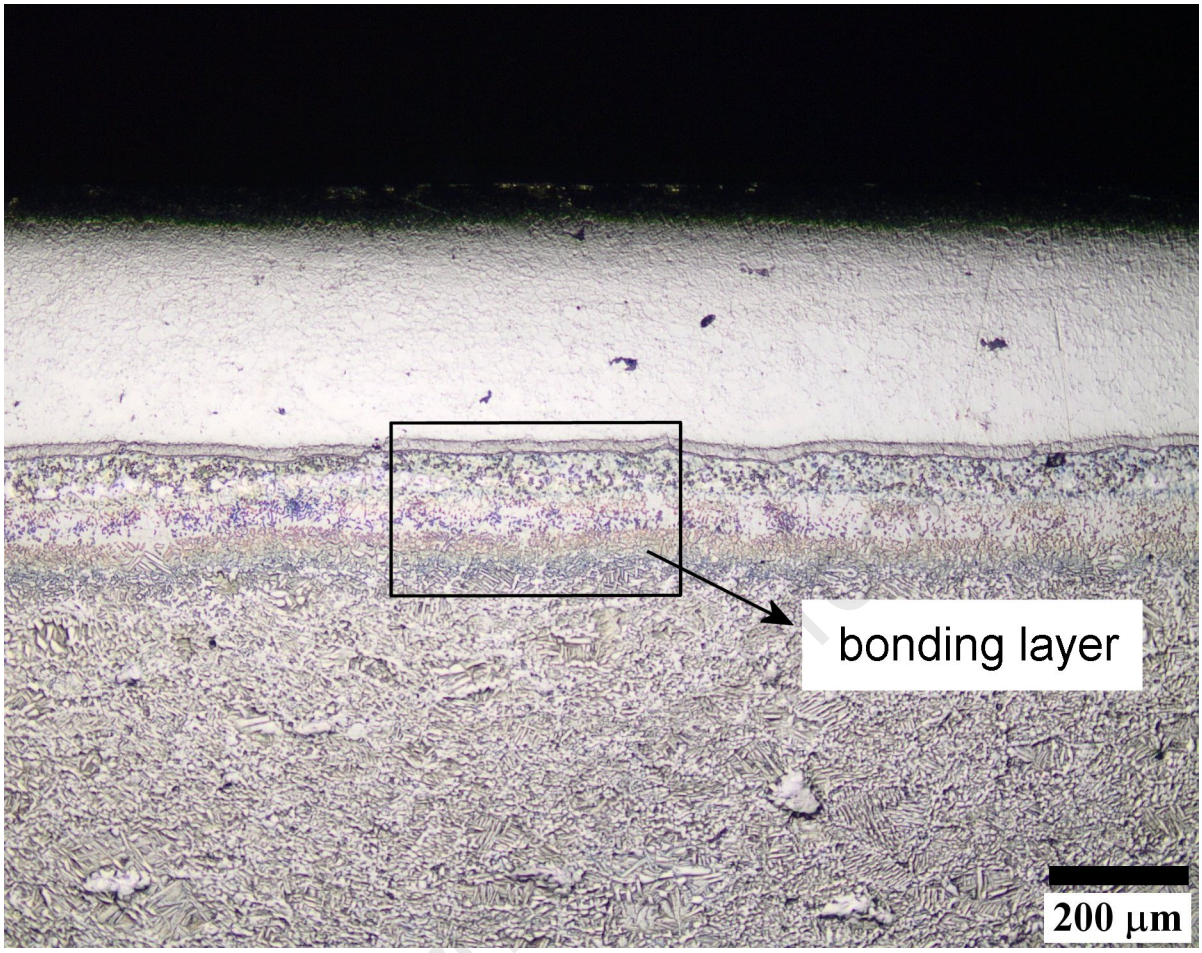

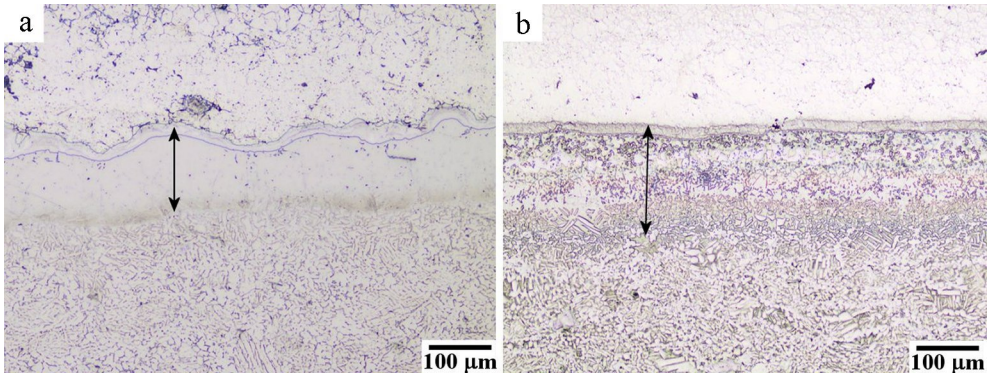

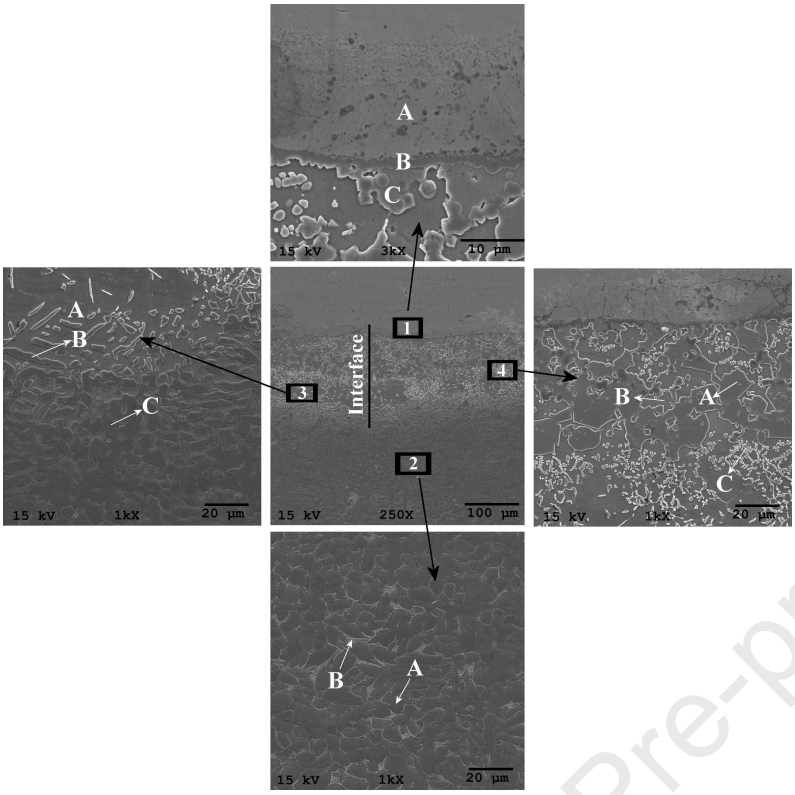

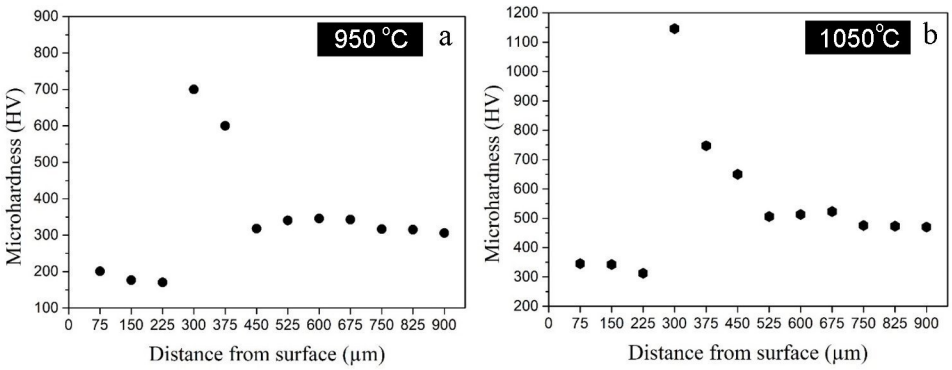

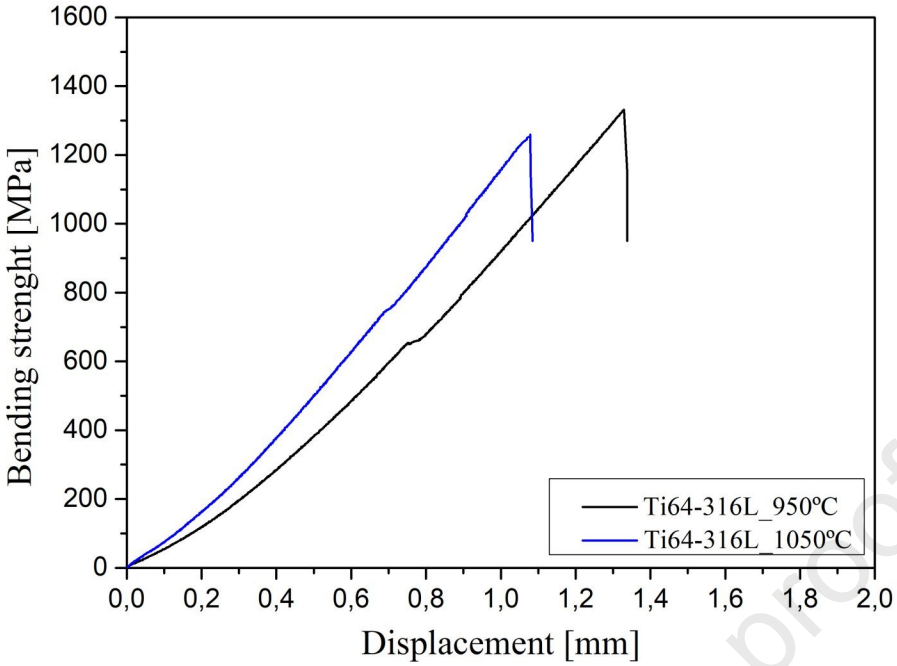

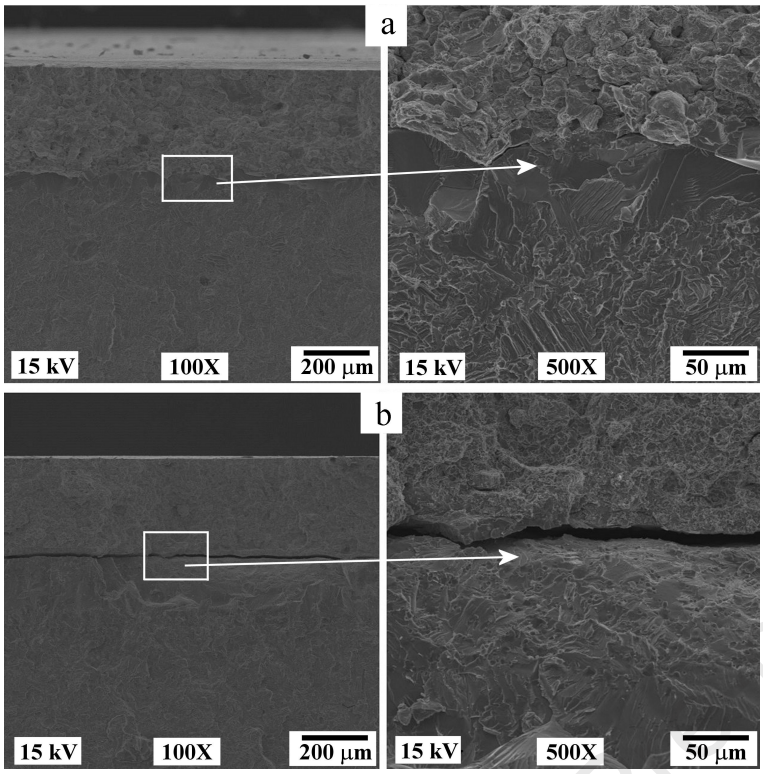

CRediT author statement

Fuad Khoshnaw: Investigation, Methodology, Validation, Writing - Original Draft, Review and Editing
Ridvan Yamanoglu: Methodology, Validation, Writing - Original Draft, Supervision
Umit Gencay Basci: Investigation, Methodology, Editing
Onur Muratal: Investigation, Methodology

Declaration of interests

☒ The authors declare that they have no known competing financial interests or personal relationships that could have appeared to influence the work reported in this paper.

☐The authors declare the following financial interests/personal relationships which may be considered as potential competing interests:

Dr. Rıdvan YAMANOGLU
Corresponding Author